Verification of chaotic behavior in an experimental loudspeaker

Joshua D. Reiss
*Department of Electronic Engineering, Queen Mary, University of London, Mile End Road, London E14NS,
United Kingdom*

Ivan Djurek[a] and Antonio Petosic[b]
*Department of Electroacoustics, Faculty of Electrical Engineering and Computing, University of Zagreb,
Unska 3, Zagreb, Croatia*

Danijel Djurek[c]
*Alessandro Volta Applied Ceramics, (AVAC) Laboratory for Nonlinear Dynamics, Kesten brijeg 5, Remete,
Zagreb, Croatia*

The dynamics of an experimental electrodynamic loudspeaker is studied by using the tools of chaos theory and time series analysis. Delay time, embedding dimension, fractal dimension, and other empirical quantities are determined from experimental data. Particular attention is paid to issues of stationarity in a system in order to identify sources of uncertainty. Lyapunov exponents and fractal dimension are measured using several independent techniques. Results are compared in order to establish independent confirmation of low dimensional dynamics and a positive dominant Lyapunov exponent. We thus show that the loudspeaker may function as a chaotic system suitable for low dimensional modeling and the application of chaos control techniques.
© 2008 Acoustical Society of America. [DOI: 10.1121/1.2967843]

I. INTRODUCTION

Loudspeakers are the most variable elements in any audio system and are responsible for marked audible differences between otherwise identical sound systems. The performance of loudspeakers (i.e., their accuracy in reproducing a signal without adding distortion) is significantly poorer than that of other audio equipments. For example, harmonic distortion in a typical loudspeaker can be 100 to 1000 times greater than that of amplifiers.[1] The frequency response of a loudspeaker is often referenced as being within ± 3 dB of perfect linearity (and many speaker designs fall further outside this range), whereas that of an amplifier may vary by less than 0.1 dB. Thus an improved understanding of the dynamics of a loudspeaker is of great importance since a better loudspeaker design may yield a significantly better performance in an audio playback system.

In a dynamic loudspeaker, sound is typically reproduced by the movement of a current-carrying object in a magnetic field due to the Lorentz force. An electrodynamic loudspeaker, as depicted in Fig. 1, is a type of a dynamic loudspeaker in which the magnetic field is produced by a permanent magnet. The audio signal from the amplifier, which is a time-varying voltage, causes a current to flow through a tightly wound coil of wire called the voice coil. The voice coil is attached to a stiff but light cone and connected to a fixed chassis by means of a flexible membrane. The spider, a weblike membrane, suspends the voice coil in the center of

the magnet and provides part of its restoring force. The surround connects the cone to the speaker chassis and keeps nonaxial motion to a minimum so that the cone functions approximately as a rigid piston. The interaction of the coil and the driver's magnetic system generates a mechanical force that causes the coil, and thus the attached cone, to move back and forth. This creates pressure waves in the air, which reproduce the original audio signal coming from the amplifier as sound.

A simplified model of an electrodynamic loudspeaker operates as a driven damped harmonic oscillator.[2] The dynamics of the displacement of the membrane, x, is given by the second order time-dependent ordinary differential equation

$$M\frac{d^2x}{dt^2} + R_M\frac{dx}{dt} + kx = BlI_0\cos(\omega t), \qquad (1)$$

where M is the combined mass of the membrane and voice coil, k is the elastic stiffness, B is the magnetic field, l is the length of the voice coil wire, and I_0 represents the drive current with frequency $f_0 = \omega_0/(2\pi)$. The friction term R_M consists of internal membrane friction and friction coming from vibration in air. Note that this model is not used in the analysis of the experiment but is given in order to show the need for higher order nonlinear terms to accurately represent the dynamics.

Both an inhomogeneous magnetic field and the excursion-dependent stiffness of the suspension account for the nonlinear behavior of the transducer. Thus, all coefficients in Eq. (1) are dependent on displacement x. The mass M was measured by weighing the detached vibrating parts and was found to be 13.1 g. However, due to the elastic

---

[a]Electronic mail: ivan.djurek@zg.t-com.hr
[b]Electronic mail: antonio.petosic@fer.hr
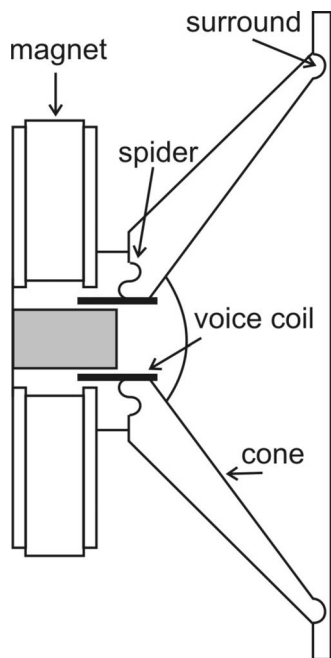[c]Electronic mail: danijel.djurek@zg.t-com.hr

FIG. 1. Diagram of an electrodynamic loudspeaker.

FIG. 2. Experimental setup with a loudspeaker and a laser distance meter.

properties of the membrane, which spans between the voice coil and the suspension on the perimeter, M should be replaced by an effective mass, M_{eff}. M_{eff} was evaluated from the Q-factor of the loudspeaker[3,4] and, as expected, was found to be dependent on displacement. For higher driving currents, the parameter Bl decreases with displacement nearly symmetrically relative to a zero position.[5] In these experiments, $Bl=3.9$ T m and reduces to ~3.6 T m for a membrane displacement of ±6 mm, and corresponding nonlinearities can be neglected. In most commercially available loudspeakers, the elastic stiffness has a quadratic dependence on displacement. A systematic approach to describing such a vibrating system, using the Duffing equation, was provided by Woafo,[6] where it was shown that related models of electromechanical transducers may exhibit chaos. However, Woafo also noted that a linear version is used to describe loudspeakers and that nonlinear terms, which are known to cause subharmonics, are often neglected.[6,7]

The stiffness was recorded in static measurements by the use of calibrated loads and corresponding measurements of the membrane deflections and may be given as approximately $k=m+nx+px^2$, where $m=480$ N m^{-1}, $n=31$ N m^{-2}, and $p=7.5$ N m^{-3}. Due to the viscoelastic contribution of the membrane polymer material, this disagrees substantially with the stiffness calculated in the dynamic regime from the simple resonance formula $\omega=k/M$, even in the regime of comparatively small drive currents ($I_0<100$ mA). Thus higher order corrections coming from the dynamics of a vibrating viscoelastic body[8,9] must be included.

When dealing with moderately low driving currents, a significant agreement was found between a model based on static measurements and the experimental data, especially for an estimation of frequency dependence and electrical impedance under a variety of different operating regimes.[10] Although simple models can be used to identify loudspeaker
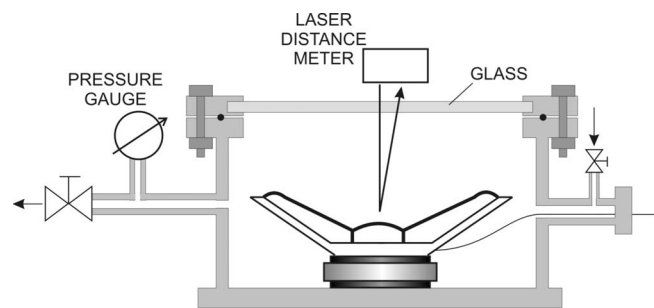
parameters, at high drive currents ($I_0>1$ A) they generally do not account for the rich nonlinear dynamic behavior that might be observed.[11–13]

Evidence of a possible chaotic behavior in a loudspeaker was first observed by Wei et al. in 1986,[14] where the appearance of subharmonics and broadband spectra at various drive frequencies and voltages was noted. Recent work strengthened this conjecture,[15–17] with the observation of hysteresis and period doubling when the loudspeaker was driven at low frequencies. This, in general, is not observed in the models. Thus it is important to verify chaos and adjust the models accordingly.

In this work, we analyze time series from an experimental electrodynamic loudspeaker system. We use a variety of techniques from the chaotic time series analysis[18] to show that the system is indeed chaotic and exhibits low dimensional dynamics suitable for further analysis and the implementation of chaos control techniques. By quantifying the nonlinear behavior, we also provide empirical observations, which may be used to refine the modeling and design of loudspeakers.

II. EXPERIMENTAL SETUP

In these experiments, a low frequency loudspeaker was used with a resonant frequency, recorded in air, of $f=38$ Hz, driving current of $I_0=10$ mA, factor of $Bl=3.9$ T m, membrane diameter of $2R=16$ cm, rated rms power of 60 W, and nominal impedance of 8 Ω. According to the manufacturer's data, the voice coil inductance is $L=0.9$ mH, and the contribution of the inductive part ωL to the loudspeaker's impedance can be neglected for driving frequencies $f<100$ Hz.

The experimental setup is depicted in Fig. 2. The loudspeaker was placed in a stainless steel chamber. Air pressure within the chamber was measured by the use of an absolute capacitive gauge with an ultimate resolution of 0.01 mbar. A glass window on the top of the chamber ensured the transparency to the light beam from the laser distance meter, which measured the vibration amplitude with an accuracy of 2 μm and a sampling frequency of ~1 kHz (a similar measurement apparatus was used to analyze nonlinear vibrations of a loudspeaker in Wei et al.[14]). The analog/digital (A/D) converter resolution of the laser distance meter was 8 bits. This allowed the acquisition of 128 amplitude levels in both up and down vibration directions. In order to check the possible influence of the chamber wall friction on the course of
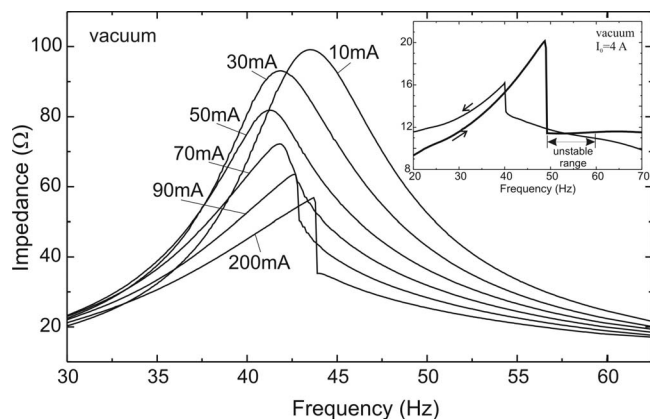
FIG. 3. Impedance measured *in vacuo* for various driving currents. The inset shows the hysteresis of the cutoff frequency for positive and negative frequency sweeps.
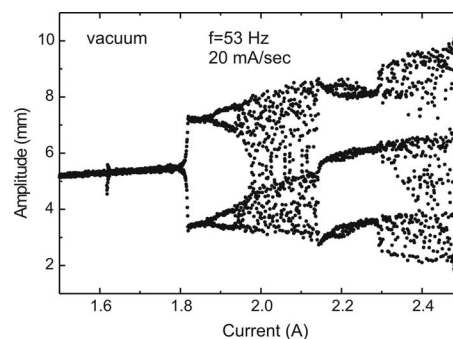

FIG. 4. A bifurcation diagram of vibration amplitudes recorded *in vacuo* for a fixed driving frequency of 53 Hz and a sweeping driving current of 20 mA/s.

measurements, the impedance and vibration amplitude data were recorded at 1 bar air pressure in a closed chamber and compared to those evaluated in free laboratory atmosphere. In a frequency range near 50 Hz, recorded data, notably impedance, showed no significant difference.

For impedance and amplitude measurements, the loudspeaker was connected to an audio amplifier with a rated power of 300 W via a series resistor 0.44 Ω. A rather small resistor value was used because of the possibility of driving higher currents. However, small resistance gave rise to increased influence of the back electromotive force. A satisfactory compromise was found with the total voltage swing across the loudspeaker, clipping not included, of ± 50 V, which, in turn, provided driving currents $I_0 = 4-5$ A. For driving currents $I_0 < 100$ mA, the back electromotive force is comparable to the friction term in Eq. (1), while for higher currents intrinsic friction increased and became the dominant contribution to the impedance.

The loudspeaker vibration amplitude dependent on frequency was measured for various driving currents in an evacuated space and in normal atmospheric pressure (1 bar).[19] The data recorded *in vacuo* are shown in Fig. 3. By an increase in the driving current, the resonance curve became more and more distorted until an amplitude downturn (cutoff) appeared near $f = 43.5$ Hz for $I_0 = 200$ mA. This current indicated the starting value for an identification of the chaotic regime. The inset in Fig. 3 depicts the hysteretic property of the cutoff effect. That is, cutoff frequencies differ for positive and negative frequency sweeps.

The onset of the amplitude cutoff was followed by a subsequent frequency sweep, which gave rise to the erratic vibration amplitude. This unstable range extended up to 54 Hz. This was chosen as the fixed frequency for an evaluation of the appearance of subharmonics that precede the chaotic state. An important feature of the unstable range was the relatively small change in the impedance with increasing driving current. In these experiments, loudspeaker impedance stayed at ~ 11 Ω, irrespective of whether the system was operated in air or in an evacuated chamber. This, in turn, meant that the driving system could be considered as a current source, even in the case when the amplifier was used as a voltage source.

A bifurcation diagram, as shown in Fig. 4, was produced by fixing the frequency at $f = 53$ Hz, sweeping the driving current at $I_0 = 1.5-2.5$ A at a rate of 20 mA/s, and recording the amplitude of the displacement of the loudspeaker. At $I_0 \sim 1.81$, a first bifurcation pitchfork appeared, which was followed by multiple period doublings, until at $I_0 = 2.15$ A the characteristic period 3 window appeared[20] and the system vibrated with three amplitudes. The existence of period doubling and a period 3 window was a strong indicator of chaos.

However, the period 3 window was observed only in an evacuated space, and data from a loudspeaker operating in an evacuated chamber are unsuitable for time series analysis techniques. This is primarily because the voice coil bonding agent evaporates when in a vacuum, which, in turn, changes the resonant frequency during the course of the measurements. In addition, for a long time and heavy duty loudspeaker operation, it is important to remove heat from the loaded voice coil, and this is more easily accomplished in an air atmosphere.

Measurements in 1 bar air were performed in a closed chamber since this minimized parameter drift due to free air convection in the laboratory. The driving frequency was fixed at 56 Hz, and the driving current was increased up to values when higher harmonics appeared as a result of the nonlinear restoring term in Eq. (1). Excerpts of the time series waveforms representing various driving currents are given in Fig. 5. Figure 5(a) shows the time-dependent vibration amplitude at the starting driving current $I_0 = 2.4$ A when the recorded signal shows a nearly sinusoidal behavior. Figures 5(b)–5(d) show new vibration amplitudes (marked with triangles), which appear with increasing driving current. The corresponding averaged spectra over the whole time series are given in Fig. 6. Figure 6(a) shows the expected behavior, with a fundamental frequency corresponding to the drive frequency. The first subharmonic appeared at 28 Hz, as depicted in Fig. 6(b). A further increase in the driving current resulted in a new subharmonic at 14 Hz [see Fig. 6(c)] and a subsequent appearance of broadband behavior, [Fig. 6(d)].

The bifurcation diagram for measurements of vibration amplitude in air is shown in Fig. 7 and was produced in the same manner as Fig. 4. Vertical lines indicate values of driving currents for which the Feigenbaum ratio $\delta_1/\delta_2 = 4.669$ is fulfilled.[21] A period 3 window cannot be seen, but this is not a contra-indicator of chaos. Noise in the data acquisition sys-

J. Acoust. Soc. Am., Vol. 124, No. 4, October 2008

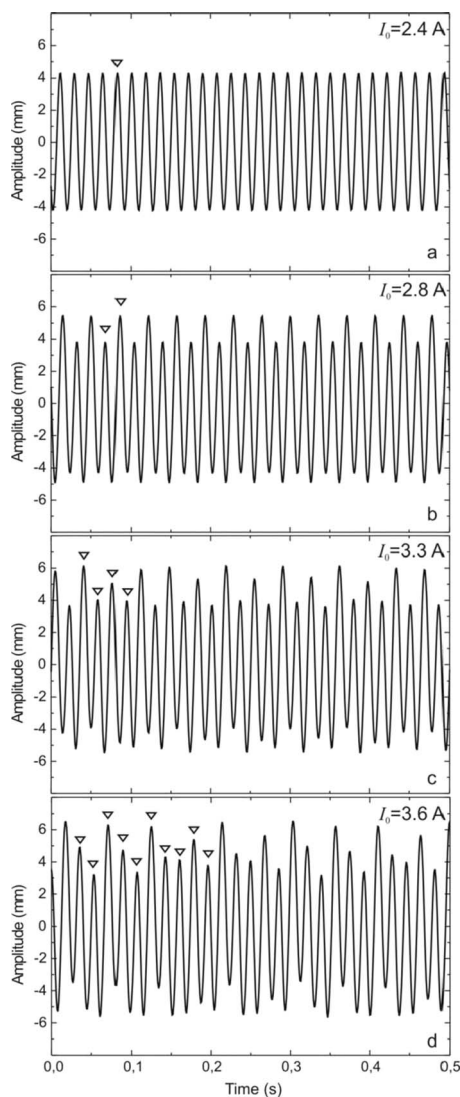Reiss *et al.*: Loudspeaker chaos   2033

FIG. 5. Short time series plots of the vibration amplitude recorded in 1 bar air for a fixed driving frequency of 56 Hz and various driving currents. The triangles indicate the appearance of a broadband behavior.

FIG. 6. Average spectrum of vibration amplitude recorded in 1 bar air for various driving currents corresponding to those in Fig. 5.

tem may obscure the window, and the existence of such a window is not considered a necessary condition. Whereas heating the voice coil makes long term measurements difficult for the evacuated loudspeaker experiment, reverberation and air circulation added noise to the short term measurements used in generating the bifurcation diagram of Fig. 7.

Leaving the loudspeaker to operate at a driving frequency of 45 Hz, the driving current was selected at a value slightly below 2.8 A, at which point the first subharmonic became attenuated. This indicated the starting point for recording the vibration amplitude included in a time series analysis. A rather low frequency of 45 Hz was selected because the dynamics appeared less susceptible to parameter drift and nonstationary behavior in this range.

The time series analysis presented in the following sections is derived from a 247 392 point experimental flow data set. The data were recorded with a 16 bit resolution, although this is further limited by the 8 bit resolution of the laser distance meter. The sample rate was 1024 Hz, so that the data set is just over 4 min long and there are approximately
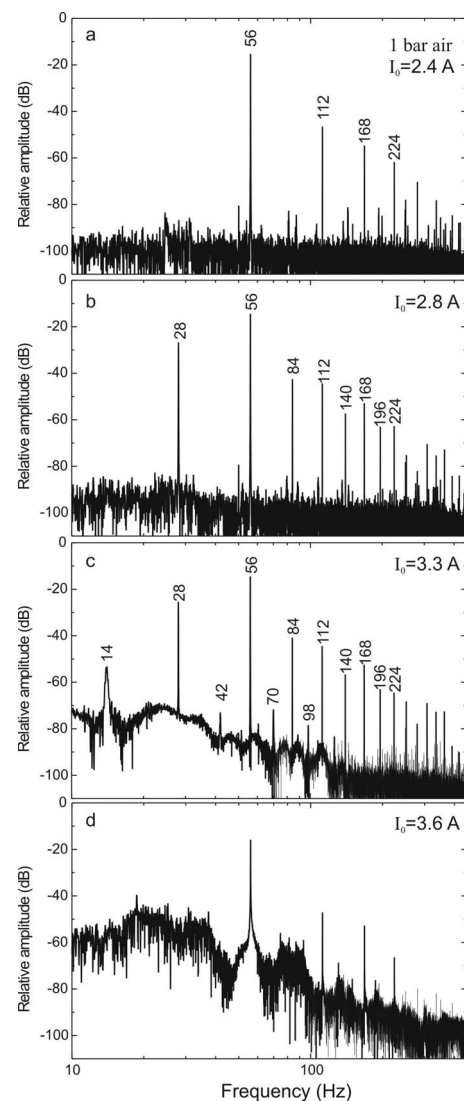
22.76 samples per drive period. In the results that follow, units are not typically given on the measurements since they have been scaled and transformed by the data acquisition system.

III. DATA ANALYSIS AND RESULTS

To analyze a one dimensional experimental data set using chaotic time series analysis techniques, it is necessary to
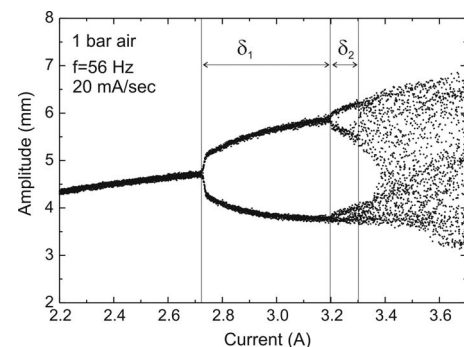

FIG. 7. A bifurcation diagram of vibration amplitudes recorded in 1 bar air for a driving current swept at 20 mA/s and a fixed driving frequency of 56 Hz.

Reiss *et al.*: Loudspeaker chaos

transform the data using phase space reconstruction techniques. If only one variable from the system can be observed, $\mathbf{X} = \{X(1), X(2), \ldots, X(N), \ldots\}$, then a D dimensional time series of length N, $\mathbf{Y} = \{Y(1), Y(2), \ldots, Y(N)\}$ is constructed from the original time series using a delay d as follows:

$$\mathbf{Y}(n) = (X(n), X(n+d), \ldots, X(n+(D-1)d)), \quad (2)$$

where we have assumed that $\mathbf{X}$ contains at least $N + (D-1)d$ data points. If the time between samples represents one period of data, then $\mathbf{X}$ represents a time series generated from a map, or a Poincaré section of the system, in which case the delay d used to generate $\mathbf{Y}$ is usually set to 1.

Assuming that the time series is stationary, that is, the parameters that govern the dynamics are not significantly changing over time, then with sufficient data and the appropriate choice of the delay parameter d and the embedding dimension D, $\mathbf{Y}$ will accurately represent the dynamical behavior of the system. Once $\mathbf{Y}$ has been constructed, then further analysis of this multidimensional time series may be used to estimate various quantities related to the structure of the phase space, such as the dimensionality of the attractor, characterization of the chaotic behavior or lack thereof, and identification of chaotic orbits.

In the following subsections, we construct delay coordinate embeddings from the scalar time series and then use this technique to analyze the data and quantify the dynamical system properties. We will use the notation introduced above to describe the original scalar time series, $\mathbf{X} = \{X(1), X(2), \ldots, X(N)\}$, and a delay coordinate embedding of the time series, $\mathbf{Y} = \{Y(1), Y(2), \ldots, Y(N)\}$.

A. Nonstationarity and long term dynamics

A few simple tests that would identify strong drifts in the data were first performed. Sliding windows of varying lengths were applied to the data, and statistical quantities such as mean, maximum, minimum, and standard deviations were computed for each window. If the data were truly stationary, then these quantities would remain constant throughout the data. The results of the drift in the maximum and minimum values of a one second window (1024 data points) are depicted in Fig. 8.

It can be seen that the dynamics of the system are not entirely stationary. For instance, the maximum value undergoes an upward trend, particularly near the beginning of the time series. This nonstationarity was also confirmed by the measurement of other statistical quantities such as the skewness and kurtosis for windowed data.

When the dynamics change over time in an experimental system, it is often difficult to determine the cause. The behavior may be caused by long term dynamics, which are inherent to the system, or by a simple transient before settling into some behavior. However, this fluctuation is quite small in relation to the full extent of the data (for instance, the variation in the maximum value is less than 2% of the full scale of the data). Thus, although it may affect the results of chaotic time series analysis methods, it is still small enough such that the data are acceptable for analysis.
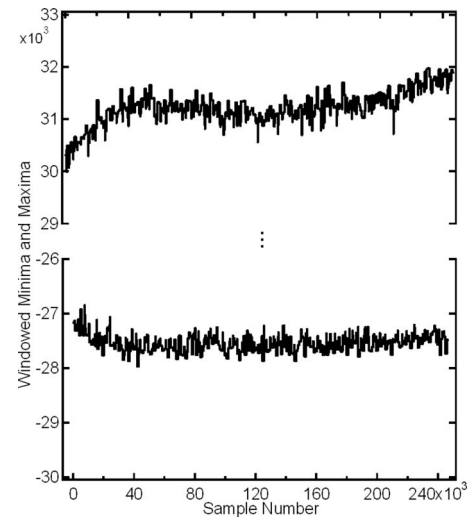

FIG. 8. Nonstationary behavior of the time series. Plotted are estimates of the maximum and minimum values for overlapping windows of 1024 samples (1 s) from the experimental data.

B. Poincaré sections

A common technique in a chaotic time series analysis is to generate a Poincaré section, with one point per period, from data sampled at a much higher frequency than the drive frequency. Given that the system has a drive frequency of 45 Hz, a natural Poincaré section would be to sample the system at the drive frequency. Since this was not possible due to the limited sampling frequencies of the data acquisition system, we considered several techniques for extracting a Poincaré section. These included the peak amplitude values, their second derivatives, times between peaks, and times at which the amplitudes cross a fixed value. Figure 9 depicts the Poincaré section plots using extracted peak amplitudes and extracted times between zero crossings in the flow data. Both techniques successfully capture the dynamics, although the use of zero crossings appears slightly less noisy.

C. Embedding parameters

A reasonable value for the delay may be suggested either by the first zero crossing of the autocorrelation function or by the first minimum of the mutual information function[22,23] as either value is plotted as a function of delay. For the time series data, given a delay d, the autocorrelation is found simply from

$$R(d) = \frac{1}{(N-k)\sigma^2} \sum_{n=1}^{N-k} [X(n) - \mu][X(n+d) - \mu], \quad (3)$$

where μ is the mean and σ^2 is the variance of the data.

The mutual information of two random variables, $a \in A$ and $b \in B$, is given by

$$I(A;B) = \sum_{a \in A} \sum_{b \in B} p(a,b) \log \frac{p(a,b)}{p(a)p(b)}, \quad (4)$$

where the convention $0 \log 0 = 0$ is used. In the case of the mutual information between a time series and a delayed version of itself, a represents a range of values for $X(n)$ and b denotes a range of values for $X(n+d)$. These values must be

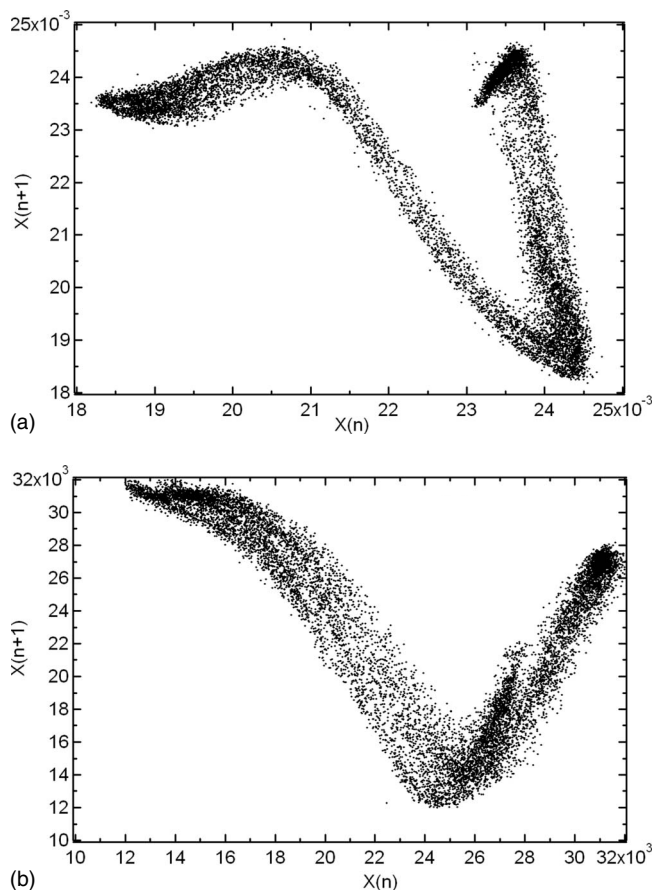FIG. 11. A two dimensional plot of the experimental data with a delay of 7.

FIG. 9. Plot of the waveform for two methods of sectioning the data. The top plot depicts peak amplitudes and the bottom plot depicts time intervals between zero crossings.

chosen so as to provide a reasonable approximation to the mutual information of the underlying dynamical systems generating $X(n)$ and $X(n+k)$. Here, the mutual information was calculated efficiently using a method described in Reiss *et al.*,[24] which partitions the range of values for $X(n)$ and $X(n+k)$ recursively until there is no more hidden structure.

The mutual information often gives a better value because it takes nonlinear correlations into account. However,

for the loudspeaker data, the mutual information function and the autocorrelation function were in strong agreement. As shown in Fig. 10, the autocorrelation suggests a delay of 6 and the mutual information suggests a delay of 7. This was in agreement with visual inspection since two and three dimensional plots revealed the most structure near these values of delay (see Fig. 11). Unfortunately, they also reveal a complexity or noise dependence that makes the fine scale structure very difficult to detect.

A modified form of the false nearest neighbor (FNN) algorithm[25] was chosen as the primary technique for determining the embedding dimension. The modification is intended to take into account stochastic phenomena, which result in FNNs occurring regardless of the embedding dimension. An appropriate embedding dimension is found when the percentage of FNNs drops to a constant value. As shown in Fig. 12, the percentage of false neighbors approaches a constant value with an embedding dimension of 5 for the flow data and an embedding dimension of 4 for either sectioned data set. This is in agreement with the observation that a Poincaré section should have one less dimension than the original data.
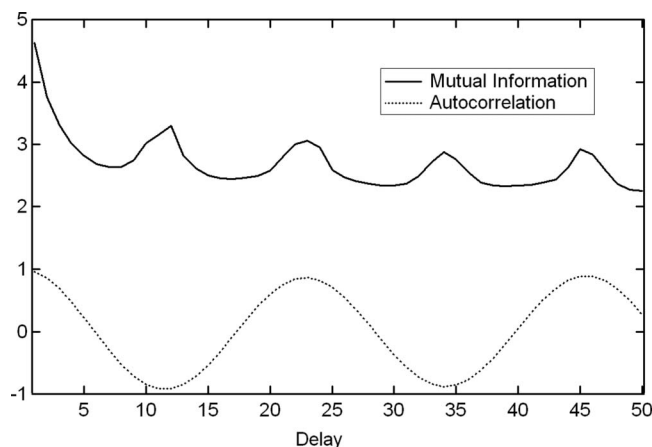

FIG. 10. Two techniques for estimating an embedding delay from the experimental data. The first method uses the first minimum of the mutual information function, and the second uses the first zero crossing of the autocorrelation function. The methods suggest a delay between 6 and 7.
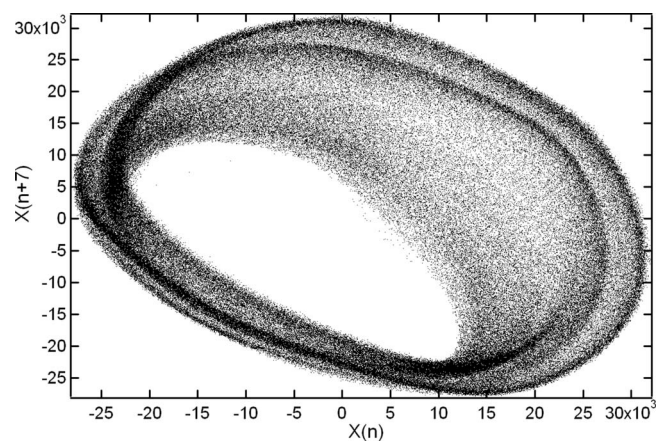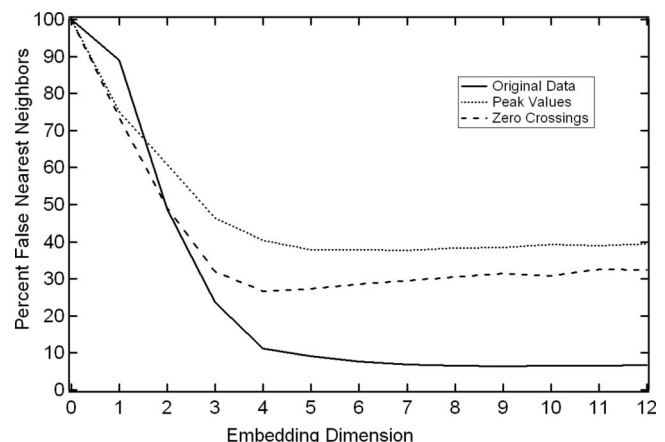

FIG. 12. Results of the FNN routine as applied to the flow data. An appropriate embedding dimension is found when the percentage of false near neighbors drops to a constant value. This indicates that the embedding dimension should be at least 4.
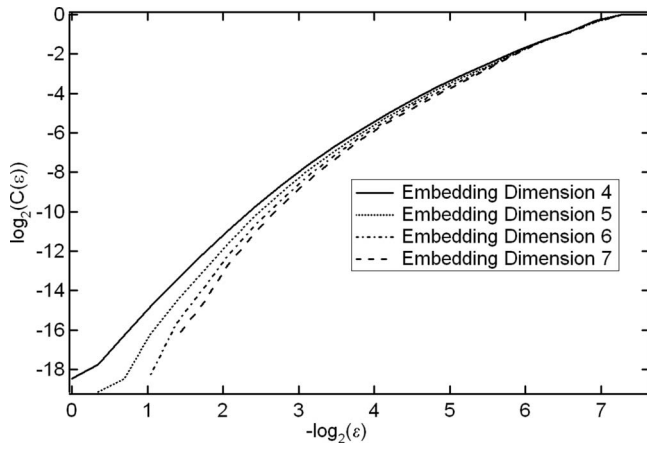
FIG. 13. Plot of the log correlation function vs log distance. With sufficient low noise data, the slope of the plot may provide the correlation dimension.

D. Fractal dimension

The dimensionality of a chaotic attractor is typically a noninteger value. That is, the attracting region of the phase space will not completely fill out a region of that space. In this section we use several different methods to estimate the dimensionality of the loudspeaker data, which further give an idea of the complexity of the underlying dynamics.

The correlation dimension is found by constructing a function $C(\varepsilon)$, which is the probability that two arbitrary points from the delay coordinate embedding are closer together than a distance ε,

$$C(\varepsilon) = \frac{2}{N(N-1)} \sum_{i=1}^{N} \sum_{j=1}^{i-1} H(\varepsilon - |Y(i) - Y(j)|), \quad (5)$$

where H is the Heaviside unit step function. The correlation dimension of an experimental time series is then given by

$$D = d \log(C)/d \log(\varepsilon) \quad (6)$$

in the limit $\varepsilon \to 0$ and $N \to \infty$. The correlation dimension may be estimated by the slope of the curve $\log[C(\varepsilon)]$ vs $\log(\varepsilon)$. A noninteger result for the correlation dimension indicates that the data are probably fractal. For too low or too high ε values, the results are inaccurate, so the slope must be measured in the midrange of the curve. A good value should be in the region where measurements of the dimension are most stable.

The Grassberger–Proccacia algorithm,[26,27] was used to estimate fractal dimensions. The results of $\log_2[C(\varepsilon)]$ vs $\log(\varepsilon)$ for the peak values from the original 45 Hz data are depicted in Fig. 13. The correlation dimension cannot be accurately estimated since there is not one significant region where the slope remains constant. This is because estimates of correlation dimension using the Grassberger–Proccacia algorithm are highly susceptible to noise and data set size. A limited data set size reduces the region of the plateau and increases uncertainty, and the presence of noise implies that an accurate measurement can only be obtained for large ε. For higher dimensional data these problems are aggravated since minimal noise and exponentially more data are required to identify the plateau region. In addition, data with a high sample rate may exhibit strong correlations that skew the estimates. The approximations due to noise, data set size, nonstationarity, and so on are inherent in the data set. However, the Grassberger–Proccacia algorithm also uses an approximation to the definition of correlation dimension. Therefore, we attempted an alternative technique that allows an estimation of the multiple definitions of the fractal dimension.

The delay coordinate embedded data can be gridded into n dimensional boxes of equal length ε, such that all vectors lie within these N boxes. If a box is labeled i, then it has an associated probability, $P_i(\varepsilon)$, that a vector on the attractor will reside within this box. The generalized entropies, $H_0, H_1, \ldots$, are defined in terms of the probabilities of vectors occupying the boxes. For $q = 0, 1, 2 \ldots$,

$$H_q(\varepsilon) = \frac{1}{1-q} \ln \sum_{i=1}^{N(\varepsilon)} P_i^q(\varepsilon), \quad q \neq 1,$$

$$H_1(\varepsilon) = - \sum_{i=1}^{N(\varepsilon)} P_i(\varepsilon) \ln P_i(\varepsilon). \quad (7)$$

In the following we keep the conventions common in dimension definitions and use the natural logarithm as opposed to log base 2. The generalized dimension of order q is then defined as

$$D(q) = - \lim_{\varepsilon \to \infty} \frac{H_q(\varepsilon)}{\ln \varepsilon}. \quad (8)$$

Under this definition, $D(0)$, $D(1)$, and $D(2)$ are the box counting dimension, the information dimension, and the correlation dimension, respectively. We also have the property that if $p > q$, then $D(p) \leq D(q)$.

Once the generalized entropies have been determined, there are two ways to approximate the generalized dimensions for time series data. The first is if ε is sufficiently small such that the limit is approximately correct and we have enough data to get an accurate measurement for $H_q(\varepsilon)$. In that case we may use

$$D(q) = D_q(\varepsilon) = - H_q(\varepsilon)/\ln \varepsilon. \quad (9)$$

However, the preferred method is to simply look at the slope of a plot of $H_q(\varepsilon)$ vs $\ln(\varepsilon)$ since this has a quicker rate of converge to the limit of $\varepsilon \to 0$. We should mention that further information on theoretic properties can be determined from the analysis of this sorting, such as the generalized mutual information of high dimensional data, $I_n(X_1, X_2, \ldots, X_n)$, or the estimation of the metric entropy.[28]

For a large box size, the box counting dimension varies widely from the others since the box counting dimension $D(0)$ is more susceptible to errors. It is also a poor quantity to use since it says nothing about the density of the attractor, only about its shape. However, the box counting dimension and all the others converge in the midregion before diverging slightly and then dropping to zero (due to data set size). It is this midregion that parallels the plateau region of the Grassberger–Proccacia algorithm.[26,27]

J. Acoust. Soc. Am., Vol. 124, No. 4, October 2008

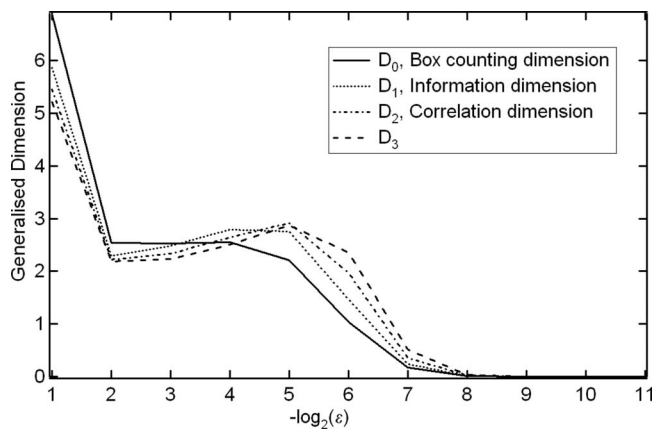Reiss *et al.*: Loudspeaker chaos   2037

FIG. 14. Plot of the first four generalized dimensions from the original data.

Figures 14 and 15 present the results of our calculations of the first four generalized dimensions performed on the flow data embedded in five dimensions and the sectioned data embedded in four dimensions, respectively. Displayed are estimates of the first four generalized entropies for varying box sizes. Additional tests were also performed for the embedding dimensions of 3–6 and for the next four generalized entropies. The results indicated that for $p > q$, $D(p) \leq D(q)$, which agrees with the theory.

The estimates for fractal dimension were derived from where the slope of of $H_q(\varepsilon)$ vs $\ln(\varepsilon)$ showed the least deviation for successive values of ε ($\varepsilon = 2^{-4}$ and 2^{-5}). Estimates ranged from 1.8 to 2.2 for all fractal dimensions calculated on the sectioned data and from 2.6 to 3.0 for all fractal dimensions calculated on the flow data when the embedding dimension was greater than or equal to 4. In both cases the estimate agrees with our choice of the embedding dimension and is also in rough agreement with the result from the Grassberger–Proccacia algorithm. However, in general, the dimensionality of the sectioned data is less than 1 plus the dimensionality of the flow data. This may be accounted for primarily by the small data set size for the sectioned data (approximately 10 000 points), which is known to cause a slight overestimation of fractal dimension, and the relatively high sample rate of the flow data, which skewed estimates downward.[29]
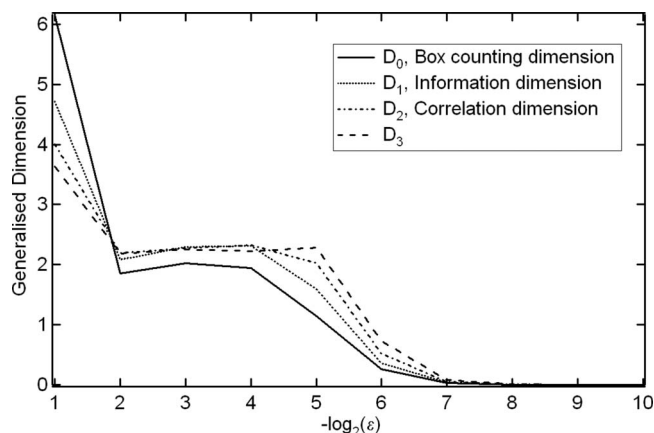

FIG. 15. Plot of the first four generalized dimensions from the sectioned data.

E. Lyapunov exponents

The Lyapunov exponents characterize how chaotic a system is. For a D dimensional dynamical system, consider the infinitesimally small D-sphere centered around a point on the attractor. As this evolves, the sphere will become a D-ellipsoid due to the deforming nature of the attractor flow. Then the ith Lyapunov exponent is defined in terms of the exponential growth rate of the ith principal axis of the ellipsoid,

$$\lambda_i = \lim_{t \to \infty} \frac{1}{t} \ln \frac{p_i(t)}{p_i(0)}. \tag{10}$$

Thus the spectrum of Lyapunov exponents, $\{\lambda_1, \lambda_2, \ldots, \lambda_D\}$ describes the rate of growth of the distance between nearby trajectories in phase space. Chaos is often defined by the existence of a positive dominant Lyapunov exponent, which indicates that nearby trajectories will, over time, diverge exponentially away from each other.

The determination of Lyapunov exponents from noisy experimental data is a difficult task. Although many methods have been presented, there are also numerous examples of these methods breaking down when tested against real data, as well as questions concerning the validity of the methods. Thus the results of exponent determination were held to scrutiny. Criteria were established for the identification of Lyapunov exponents.

There should be an agreement between exponents as measured from different algorithms, and some measurement of error should be provided. Embedding parameters used in estimating exponents must be confirmed independently by other methods. The results should remain consistent under various parameter settings for exponent estimation. For flow data, a zero exponent should be clearly found. The estimation of exponents from both flow and sectioned data should be in agreement. The sum of all the exponents must be negative, and the sum of the positive exponents should be less than or equal to the metric entropy. In fact, for many cases they should be equal.[30] Under the proper conditions, the Lyapunov exponents should all, approximately, switch sign when measured from a time reversal of the data.[31]

The Lyapunov dimension may be defined as

$$D_\lambda = L + \frac{1}{|\lambda_{L+1}|} \sum_{j=1}^{L} \lambda_j, \tag{11}$$

where L is the maximum integer such that the sum of the L largest exponents is still non-negative. That is, $\Sigma_{j=1}^{L} \lambda_j \geq 0$ and $\Sigma_{j=1}^{L+1} \lambda_j < 0$. The Kaplan–Yorke conjecture[32] proposes that this is equal to the information dimension. Within error bounds, this seems to be true. Therefore, a final criterion is that the Lyapunov dimension estimates should agree with the information dimension estimates.

It is doubtful that all criteria can be satisfied unless one is dealing with a long noise-free time series of low dimensional simulated data. Noise, high dimensionality, and short time series length (few orbits or a small number of points or both) negatively affect all methods of analysis. Some criteria, such as the confirmation of embedding parameter choices, are a virtual necessity before any calculation is made. Others,

Reiss *et al.*: Loudspeaker chaos

TABLE I. Results of the estimation of the Lyapunov exponent(s) using three different techniques. All calculations were performed with a four dimensional embedding of the peak value data.

Algorithm	λ_1	λ_2	λ_3	λ_4	Sum
Rosenstein *et al.*	0.403				
Wolf *et al.*	0.391				
Eckmann–Ruelle	0.380	0.054	−0.184	−0.484	−0.234

such as the agreement between the Lyapunov and information dimension, are very strong indicators that Lyapunov exponents have been reasonably determined. Still other criteria require calculations of quantities that are particularly difficult to compute from time series, such as metric entropy. Previous authors chose to reject the use of estimated Lyapunov exponents as discriminating statistics.[33]

Three methods of determining Lyapunov exponents were implemented: the method of Eckmann and Ruelle[34] for determining the Lyapunov spectra and the methods of Rosenstein *et al.*[35] and Wolf *et al.*[36] for determining the largest exponent. Since these methods are fundamentally different, one would not expect an agreement between the estimates to be simply due to them incorporating the same mistakes. The sectioned data were used for all estimates since these reduce dependence on the choice of delay time. Abarbanel's method was also applied,[37] although this is based on the same technique as Eckmann and Ruelle's method and the sectioned data provide very similar results.

Wolf *et al.*[36] defined the exponents in terms of the rates of divergence of volumes as they evolve around the attractor. The method of Wolf *et al.* involves following a trajectory in its path around the attractor. The rate of growth between points on this trajectory and a nearby trajectory is used to estimate the largest Lyapunov exponent. When the distance between these trajectories becomes too large, then a new nearby trajectory is found that is within a reasonable angular distance from the previous nearby trajectory. In order to minimize parameter dependence, we used a variation on the method of Wolf *et al.*[29] In previous work,[36,38,39] both maximum allowable displacement and maximum angular displacement were left as free parameters. We use one parameter: the number of near neighbors to consider after a given number of iteration steps.

The method of Rosenstein *et al.* involves looking at average divergence rates of nearest neighbors. It also finds the dominant exponent. The Eckmann and Ruelle method involves using a small neighborhood of points and iterating them forward to estimate the local Jacobian, and then determining the Lyapunov spectrum from the eigenvalues of the Jacobians around the attractor.

In Table I, results of exponent calculations are provided. All calculations were performed with a time delay of 1 and an embedding dimension of 4, as suggested by the FNN routine. The exponents are given in units of l/time, where the time scale is defined so that the time between samples is 1. Many more calculations were performed until a reasonable and stable parameter regime was found for all methods. In general, exponent calculations converged to within 5% of

their final value when averaging local estimates of the dominant Lyapunov exponent over only 1000 points (although the entire sectioned data set was used to find near neighbors).

Several of our criteria are determined immediately upon inspection. The dominant exponent results from all three methods provide a rough agreement. One check on the algorithm of Wolf *et al.* was calculating the average angular displacement. This was typically less than 20%, well within reasonable bounds. For the Lyapunov spectrum, the second exponent is very close to zero and the sum of the exponents is negative.

The folding of the attractor brings diverging orbits back together. So any effects of nonlinearities will most likely serve to move all exponents closer to zero. Also increasing the number of near neighbors used may underestimate the value because this allows a larger distance between neighbors. Hence a slight underestimate of the positive exponents for the Eckmann–Ruelle algorithm (and for Abarbanel's technique[37]) was expected. For the algorithm of Wolf *et al.*, the angular displacement errors are not likely to accumulate, but each error may skew the largest positive exponent downward. These assumptions are confirmed by the slightly lower estimate of the dominant exponent for the Eckmann–Ruelle and Wolf algorithms as compared to the technique of Rosenstein *et al.* which is less susceptible to these errors.

However, it was not possible to confirm all criteria. The measurement of the metric entropy is still ongoing. Sectioning the data introduced additional noise. More importantly, the uncertainty in sample values tended to dominate over the divergence on a small time scale, thus introducing errors into the measurement of Lyapunov exponents from the original flow data. Thus it was not possible to get an agreement between exponent estimates from the section and from the flow, nor was it expected. For the measurement of the Lyapunov spectrum, uncertainty in the values of other exponents meant that it was not possible to get a reliable estimate of the Lyapunov dimension. Time reversal results were also inconclusive at best. However, simulated data with the addition of noise would not usually switch the signs of the exponents under time reversal either. So the sign change of exponents when the data are reversed may not be a suitable criterion for noisy data.

F. Unstable periodic orbits

In addition to the occurrence of a positive Lyapunov exponent, a chaotic system may also be characterized by having an infinite number of unstable periodic orbits (UPOs). The identification of UPOs plays a critical role in many chaos control algorithms.[40] Most standard chaos control algorithms attempt to control the system onto a UPO while operating within the chaotic regime. Small time-dependent perturbations applied to an accessible parameter may then be used to force the system onto the stable manifold and hence enforce stability and a periodic behavior. The drive frequency is the most preferable candidate to use as the varied parameter in a control scheme. This is because it is easily adjustable, and a small change in drive frequency often yields appropriate changes in the dynamics. It is useful in

J. Acoust. Soc. Am., Vol. 124, No. 4, October 2008

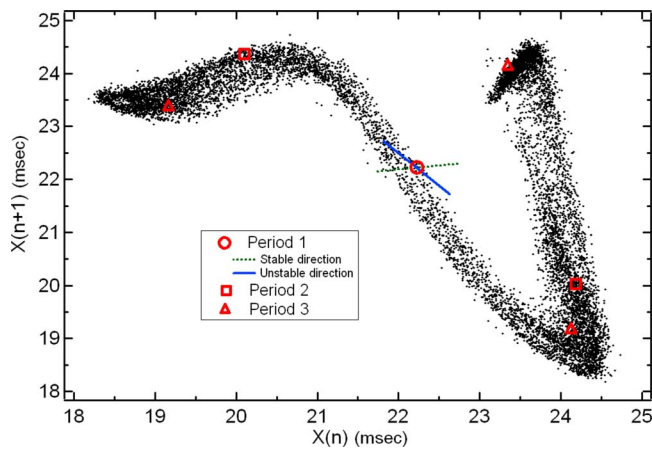Reiss *et al.*: Loudspeaker chaos   2039

FIG. 16. (Color online) A delay coordinate embedding plot of the times between zero crossings. Periods 1–3 points are identified, along with the stable and unstable manifolds of the period 1 orbit.

occasional proportional feedback control schemes in tracking and targeting of trajectories, and in the identification of symbolic dynamics.[40,41] Thus we will also attempt to characterize the UPOs exhibited during the chaotic state.

By looking for when the dynamics approach the same region after a given number of iterates, periodic orbits can be found. UPOs of period p are found simply by establishing a threshold ε,

$$\|Y(n) - Y(n+p)\| < \varepsilon, \tag{12}$$

in which case a periodic orbit exists in the vicinity of $Y(n)$ and a least squares fit of all data in the region can be used to estimate its exact location. The exact value of ε may be varied depending on the size of the data set, the period p, and the number of UPOs that one wishes to find. False positive UPOs may be identified using the mean squared error of the least squares fit.

Figure 16 shows the delay coordinate embedding of the Poincaré section using times between zero crossings. In this figure, we identified period 1, period 2, and period 3 orbits. From the least squares fit estimate of the local dynamics, the eigenvalues and eigenvectors corresponding to the stable and unstable manifolds can be found. For the period 1 orbit, we have a fixed point located at 0.0222 s, corresponding to the drive frequency of the system, 45 Hz. Its eigenvalues are 0.155 and −1.571, with corresponding eigenvectors (1,0.155) and (−0.637,1). Similar results can be obtained for other identified periodic orbits, and these results can be used to implement a chaos control technique.

IV. FURTHER ANALYSIS AND CONCLUSIONS

An analysis was attempted on time series data from an experimental electrodynamic loudspeaker in order to characterize the embedding dimension, the fractal dimension, the Lyapunov exponents, and the UPOs. The obtained results indicate that the system is governed by low dimensional chaotic dynamics and thus is highly amenable to control, tracking, synchronization, noise reduction, and so forth. Particular care was made in verifying the presence of a positive Lyapunov exponent.

Various estimates of fractal dimension were performed, including the measurement of correlation dimension,[26,27] information dimension, and box counting dimension for different embedding dimensions. Although there was qualitative confirmation of low dimensional behavior, consistent results for quantitative values for the fractal dimension were not achieved.

However, the estimation of the dominant Lyapunov exponent, which is less reliant on a large data set size, provided consistent results regardless of the method of estimation.[10] We used several different techniques that provided a rough agreement in their estimates of the dominant exponent, and the results further agreed with the theory concerning the Lyapunov spectrum and its properties. They reliably showed evidence of a positive Lyapunov exponent, a strong indicator of chaos.

Finally, we attempted to estimate the eigenvalues and eigenvectors associated with detected UPOs. These may be easily identified. Control may be applied to allow the loudspeaker to operate as desired within the chaotic regime. Tracking and maintenance should also be possible since the appropriate dynamics have been found for the application of several well-known algorithms.

However, extraction of many empirical quantities, particularly fractal dimension, proved difficult due to a number of issues. This may be accounted for partly by the nonstationarity and short data set size. Although the original data set is over 200 000 points, it represents about 10 000 orbits. This is insufficient for an effective calculation of fractal dimension in the presence of noise and long term dynamics. Furthermore, although the dynamics are somewhat stable, there is still a gradual change in various statistical quantities when examined using a sliding window through the data. This tends to distort various measurements. A longer data set size could capture the long term dynamics.

However, we believe that the difficulty in estimating some measures of nonlinear behavior and dimensionality is primarily due to low sample rates and low resolution due to limitations in the data acquisition system. First, the data were sampled at 1024 samples/s, or approximately 23 samples per period. A higher sampling rate would yield more accurate Poincaré sections. Alternatively, if the sampling data could be sampled at exactly the drive frequency, 45 Hz, then this would produce a natural Poincaré section. The analyzed data had a 16 bit precision, but this was further limited by the 8 bit resolution of the A/D converter of the laser distance meter. This meant that there was a significant uncertainty in the location of nearby points. Since most analyses of chaotic time series rely on an analysis of near neighbors in a locally linear region, these resulted in inaccuracies in the estimation of fractal dimension and Lyapunov exponents.

Current work is focused on improvements to the data acquisition system. This would allow a more accurate analysis of the data, including measurements of how fractal and Lyapunov dimensions change with parameter settings, and use of chaotic time series prediction methods on the data. This could also be used for further direct comparison with a dynamical behavior from enhanced models of the loudspeaker. An accurate model of an electrodynamic loud-

speaker would represent a significant advance in the field, particularly since model parameters could then be modified to yield a loudspeaker design with optimal performance.

[1] P. Klipsch, "Loudspeaker distortion," Proceedings of the IEEE International Conference on Acoustics, Speech, and Signal Processing, ICASSP '76, Philadelphia, PA, pp. 543–546.

[2] D. Davis and E. Patronis, *Sound System Engineering*, 3rd ed. (Elsevier, New York, 2006).

[3] E. S. Olsen and K. Thorbog, "Diaphragm area and mass nonlinearities of cone loudspeakers," Proceedings of the 99th AES Convention, New York, 1995, Convention Paper No. 4082.

[4] M. Colloms, *High Performance Loudspeakers*, 6th ed (Wiley, New York, 2005).

[5] E. S. Olsen, "Nonlinear modeling of low frequency loudspeakers: A practical implementation," Proceedings of the 102nd AES Convention, Munich, Germany, 1997, Convention Paper No. 4469.

[6] P. Woafo, "Harmonic oscillations, stability and chaos control in a nonlinear electromechanical system," J. Sound Vib. **259**, 1253–1264 (2003).

[7] P. Woafo, "Stability and chaos control in electrostatic transducers," Phys. Scr. **62**, 255–260 (2000).

[8] A. Steindl and H. Troger, "Chaotic oscillations of a fluid-conveying viscoelastic tube," in *Nonlinearity and Chaos in Engineering Dynamics*, edited by J. M. T. Thompson and S. R. Bishop (Wiley, Chichester, 1994), pp. 231–240.

[9] J. Argyris, V. Belubekyan, N. Ovakimyan, and M. Minasyan, "Chaotic vibrations of a nonlinear viscoelastic beam," Chaos, Solitons Fractals **7**, 151–163 (1996).

[10] A. Petosic, I. Djurek, and D. Djurek, "Modeling of an electrodynamic loudspeaker using Runge-Kutta ODE solver," 122nd Convention of Audio Engineering Society, Vienna, Austria, 2007.

[11] T. Leishman and G. Dix, "Additional modeling details for the suspension of a moving-coil loudspeaker," J. Acoust. Soc. Am. **116**(4), 2619 (2004).

[12] R. A. Ribeiro, A. J. Serralheiro, and M. S. Piedade, "Application of Kalman and RLS adaptive algorithms to non-linear loudspeaker controller parameter estimation: a case study," IEEE International Conference on Acoustics, Speech, and Signal Processing (ICASSP), Philadelphia, 2005.

[13] M. D. Fränken and J. Wassmuth, "Passive parametric modelling of dynamic loudspeakers," IEEE Trans. Speech Audio Process. **9**, 885–891 (2001).

[14] R. J. Wei, Q. T. Tao, and W. S. Ni, "Bifurcation and chaos of direct radiation loudspeaker," Chin. Phys. Lett. **3**, 469–472 (1986).

[15] D. Djurek, I. Djurek, and A. Petosic, "Intrinsic membrane friction and onset of chaos in an electrodynamic loudspeaker," Proceedings of the 123rd Aes Convention, New York, NY, 2007.

[16] I. Djurek, A. Petosic, and D. Djurek, "Chaotic state in an electrodynamic loudspeaker controlled by gas pressure," Proceedings of the 153rd ASA Meeting, Salt Lake City, UT, 2007.

[17] D. Djurek, I. Djurek, and A. Petosic, "Chaotic state in an electrodynamic loudspeaker," Proceedings of the 122nd Convention of the AES, Vienna, Austria, 2007.

[18] H. Kantz and T. Schreiber, *Nonlinear Time Series Analysis*, Cambridge Nonlinear Science Series (Cambridge University Press, Cambridge, England, 2004).

[19] I. Djurek, D. Djurek, and A. Petosic, "Damping of an electrodynamic loudspeaker by air viscosity and turbulence," Proceedings of the 123rd

[20] Convention of Audio Engineering Society, New York, NY, 2007.

[20] T. Y. Li and J. A. Yorke, "Period three implies chaos," Am. Math. Monthly **82**, 985–992 (1975).

[21] M. J. Feigenbaum, "The universal metric properties of nonlinear transformations," J. Stat. Phys. **21**, 669–706 (1979).

[22] A. M. Fraser, "Reconstructing attractors from scalar time series: A comparison of singular system and redundancy criteria," Physica D **34**, 391–404 (1989).

[23] A. M. Fraser and H. L. Swinney, "Independent coordinates for strange attractors from mutual information," Phys. Rev. A **33**, 1134–1140 (1986).

[24] J. D. Reiss, N. Mitianoudis, and M. B. Sandler, "Computation of generalized mutual information from multichannel audio data," Proceedings of the Audio Engineering Society 110th Convention, Amsterdam, The Netherlands, 2001.

[25] M. B. Kennel, R. Brown, and H. D. I. Abarbanel, "Determining embedding dimension for phase-space reconstruction using a geometrical construction," Phys. Rev. A **45**, 3403–3411 (1992).

[26] P. Grassberger and I. Procaccia, "Measuring the strangeness of strange attractors.," Physica D **9**, 189–208 (1983).

[27] P. Grassberger and I. Procaccia, "On the characterization of strange attractors," Phys. Rev. Lett. **50**, 346–349 (1983).

[28] A. M. Fraser, "Information and entropy in strange attractors," IEEE Trans. Inf. Theory **35**, 245–262 (1989).

[29] J. D. Reiss, "The analysis of chaotic time series," Ph.D. thesis, School of Physics, Atlanta, Georgia Institute of Technology, 2001, pp. 250.

[30] J. P. Crutchfield and N. H. Packard, "Symbolic dynamics of noisy chaos," Physica D **7**, 201 (1983).

[31] U. Parlitz, "Identification of true and spurious Lyapunov exponents from time series," Int. J. Bifurcation Chaos Appl. Sci. Eng. **2**, 155–165 (1992).

[32] P. Constantin and C. Foias, "Global Lyapunov exponents, Kaplan-Yorke formulas and the dimension of attractors for 2D Navier-Stokes equations," Commun. Pure Appl. Math. **38**, 1–27 (1985).

[33] J. Theiler, S. Eubank, A. Longtin, B. Galdrikian, and J. D. Farmer, "Testing for nonlinearity in time series: The method of surrogate data," Physica D **58**, 77–94 (1992).

[34] J.-P. Eckmann, S. O. Kamphorst, D. Ruelle, and S. Ciliberto, "Liapunov exponents from time series," Phys. Rev. A **34**, 4971–4979 (1986).

[35] M. T. Rosenstein, J. J. Collins, and C. J. De Luca, "A practical method for calculating largest Lyapunov exponents from small data sets," Physica D **65**, 117–134 (1993).

[36] A. Wolf, J. B. Swift, H. L. Swinney, and J. A. Vastano, "Determining Lyapunov exponents from a time series," Physica D **16**, 285–317 (1985).

[37] H. D. I. Abarbanel, "Tools for the analysis of chaotic data," in *Nonlinear Dynamics and Time Series, Fields Institute Communications*, edited by C. D. Cutler and D. T. Kaplan (American Math. Soc., Providence, RI, 1997), pp. 1–16.

[38] A. Wolf, "Quantifying chaos with Lyapunov exponents," in *Chaos*, edited by A. V. Holden (Manchester University Press, Manchester, 1986).

[39] A. Wolf and J. Vastano, "Intermediate length scale effects in Lyapunov exponent estimation," in *Dimensions and Entropies in Chaotic Systems*, edited by G. Mayer-Kress (Springer-Verlag, Berlin, 1986).

[40] E. Schöll and H. G. Schuster, *Handbook of Chaos Control*, 2nd ed. (Wiley, New York, 2007), pp. 849.

[41] K. Mischaikow, M. Mrozek, J. Reiss, and A. Szymczak, "Construction of symbolic dynamics from experimental time series," Phys. Rev. Lett. **82**, 1144–1147 (1999).

J. Acoust. Soc. Am., Vol. 124, No. 4, October 2008

Reiss *et al.*: Loudspeaker chaos   2041